

Dual-wave cw autodyne CO₂-laser-based lidar

V.G. Goldort,¹ E.P. Gordov,² V.N. Ishchenko,¹ A.A. Kovalev,¹
G.A. Koganov,³ M.M. Makogon,⁴ H. Rutt,⁵ and R. Shuker³

¹ *Institute of Semiconductor Physics,
Siberian Branch of the Russian Academy of Sciences, Novosibirsk, Russia*

² *Institute of Monitoring of Climatic and Ecological Systems,
Siberian Branch of the Russian Academy of Sciences, Tomsk, Russia*

³ *Faculty of Physics of the Ben Gurion University, Be'er Sheva, Israel*

⁴ *Institute of Atmospheric Optics,
Siberian Branch of the Russian Academy of Sciences, Tomsk, Russia*

⁵ *School of Electronics and Computer Science, the University of Southampton, Great Britain*

Received January 25, 2005

Results of three-year work under INTAS-ESA grant 99-822 are summarized in this paper. The autodyne lidar with new version of a dual wavelength cw CO₂ laser is described. The results presented have been obtained by modeling based on solutions of semiclassical laser equations adapted for 300-km sounding range. The sensitivity of the lidar has been estimated using a phenomenological model of detection for more than 20 contaminating gases. We describe the lidar constructed around a specially developed cw autodyne laser with the enhanced performance characteristics, as well as the technique of experiments on determination of these characteristics. The tentative results of experiments quite well agree with the estimates obtained.

Introduction

The autodyning effect in lasers consists in self-induced oscillations of lasing that may occur if a fraction of laser radiation has been entered into the cavity (e.g., the radiation reflected from a target). So, in this case, the laser is not only a source of radiation, but also an efficient detector of weak radiation.¹⁻³

The main principles of parametric autodyne lidar operation have been considered in Ref. 4 and can be summarized as follows. The frequency-tuned radiation of a cw laser is directed with an optical system to a remote reflector (a building, forest, terrain elevation). The same telescope directs the reflected radiation to the laser cavity. The interaction of the generated and return waves results in a pulsed variation of the lasing power. The modulation frequency here is related to the distance to the reflector, while the modulation amplitude bears information on the radiation losses along the path. Actually, in this configuration, the lidar is an intracavity laser spectrometer.⁵

Both theoretical and experimental results prove that using a laser to record its return signal one can not only record extremely weak optical fluxes (for example, the threshold sensitivity, for a CO₂ laser, of 10⁻¹⁷ W/Hz^{1/2}, has been demonstrated Ref. 4), but also determine the optical (and polarization^{6,7}) properties of a remote reflector and track its motion using the same equipment. All this makes autodyne lidar a promising tool in remote sensing of the atmosphere and the underlying surface. High sensitivity of autodyne lidars and with no need in phase matching of the wave fronts of sounding and

received radiation (a laser cavity makes this automatically) hold out a hope for the development of this type lidars for airborne and space-based systems.

The physics of cw autodyne lidars is by now quite clear,^{2,3} while it is not the case with pulsed lasers. Pulsed laser radars are quite convenient for many applications, because these enable one to determine distance to a target by simply measuring travel time of return signals, and the short pulse duration even at a high energy (up to 10 J per pulse) allows one to ignore nonlinear interactions in the atmosphere.

Advantages of both approaches can be combined in a hybrid laser,^{8,9} where the cw and pulsed sections with the active medium share a common cavity. Such a configuration is used to amplify and heterodyne the return signal entered into the cavity tuned to a fixed longitudinal mode. The laboratory and *in situ* experiments showed a considerable amplification of the return signal.⁸

Physically such an amplification in a hybrid laser occurs due to the energy stored in both pulsed and cw sections after the pulse has been generated. This means that for the return signal, which comes to the cavity before the complete recovery of the population inversion in the cw section, the latter works as an amplifier below the self-excitation threshold. It has been proved experimentally that this amplification can reach about three orders of magnitude depending on the arrival time of the return signal. It was demonstrated earlier⁸ that this mode holds when there is a pulse "tail" (about 10 to 100 μs long) as well as when lasing in the cw section

has recovered (in about 1 ms). Numerical modeling¹⁰ shows a good agreement with the experiments for the return time below 10 μ s. In Refs. 11–13 one can find a more detailed description of the physics of autodyne lasers and their use in sensing the objects and atmospheric parameters.

The first results obtained with space-based lidars LITE (NASA) and BALKAN (IAO SB RAS) proved their usefulness in Earth observations. At present, there are several models of space-based lidars intended for determination of the atmospheric and terrain characteristics important for meteorological and environmental control applications. However, researchers mostly rely on traditional lasers used as transmitters only, which restrict potential advantages of their use. At the same time, the sensitivity achieved in laboratory experiments makes autodyne lidars quite suitable for such applications.

In this paper, we report the results of a three-year work under the project supported by INTAS grant No. 99–822 devoted to the development of a new CO₂ laser for an autodyne lidar, establishing the lowest level of detectable signals, and estimation of lidar applicability for control of atmospheric pollutants by the differential absorption method.

The model of a parametric autodyne lidar with a dual wave CO₂ laser system

Differential absorption method in application to monitoring contents of atmospheric gases implies the use of a laser system simultaneously (or at close moments in time) emitting at two wavelengths, one of which is near an absorption line center and the other one in its wing so that the absorption at the first wavelength is strong while being weak at the second one. Feasibility of the differential absorption technique in a parametric autodyne CO₂-based lidar in application to atmospheric gas analysis has been experimentally and theoretically studied earlier.^{7,14–17}

In contrast to what has been done in Refs. 6 and 12, where the dual lasing frequency was implemented in one laser, we have developed a laser system that is based on two cw single mode CO₂ lasers with the lasing lines independently tuned in the region from 940 to 1087 cm⁻¹ (Ref. 23). Lasing frequencies can be stabilized, what is especially important in providing high sensitivity of the measurements performed using the differential absorption method.¹⁸

Based on this system, we have assembled a laboratory model of the autodyne lidar. As a transmitting and receiving optics we used a Cassegrainian telescope. The calibration experiments involved tracking topographic targets (a brick wall 40 m away and a forest 200 m away) with a 2-cm long cell filled with ethylene at variable pressure placed on the propagation path. In these experiments, we used the laser lines *P*(14) (with the ethylene absorption coefficient of 31 cm⁻¹/atm) and *P*(18)

(low ethylene absorption) of the 0001–1000 band. The amplitude of radiation intensity fluctuations when the velocity of the cavity mirror motion takes its maximum is taken as the lidar signal.

The calibration curves plotted for lidar return strength as a function of ethylene pressure were almost linear (Fig. 1) for both targets.

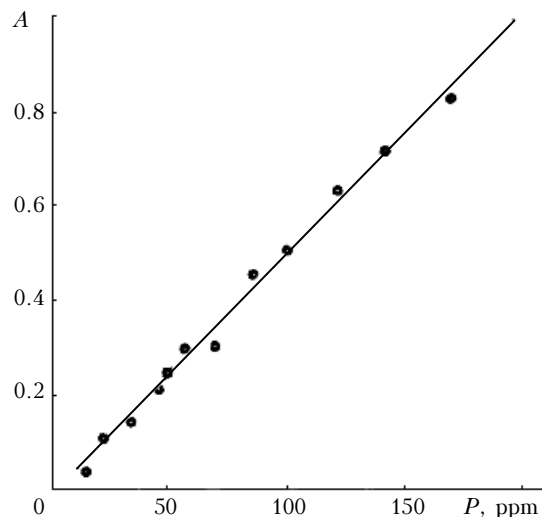


Fig. 1. The normalized lidar signal as a function of ethylene concentration in the cell; the reflector is a brick wall.

Recalculation for a 20-m thick gas layer L_g (generally not coinciding with the length of sounding path) shows that for the lowest measured normalized signal of 0.03 value, the threshold sensitivity of the autodyne lidar is about 6 ppb, which fairly well agrees with the calculations summarized in Table 2 (see below) and almost coincides with the earlier ones.¹⁴

Modeling the operation of autodyne lidar

Earlier theoretical and experimental studies of the autodyne laser were aimed mostly at elucidation of the internal laser processes. In Refs. 19 and 20 we presented an approach allowing us to analytically express such parameters as gas concentration or distance to the target, through experimentally measured parameters.

We considered the model of a parametric autodyne lidar based on a two-level laser scheme. The low reflectivity of the distant mirror (usually 10^{-9} for *in situ* experiments) allows us to obtain analytical solutions based on the perturbation theory.

Derivation of the relevant equations as well as their approximate solutions can be found in Refs. 19 and 21. The influence of atmospheric absorption along the path between the lidar and reflector on the intracavity field is taken into account by an extra reduction of the effective reflection coefficient of the exit mirror:

$$R'_0(t) = R_0 + \exp(-2\sigma CL)(1 - R_0)^2 \times \\ \times R_2 \cos\left[\frac{\omega\tau}{l}a(t) + \varphi\right], \quad (1)$$

where R_0 is the reflection coefficient of the exit mirror; R_2 is the reflection coefficient of a distant reflector; C is the concentration of the gas along the propagation path, with the absorption cross section σ ; ω is the lasing frequency; τ is the time of laser signal round trip between the lidar and retroreflector; l is the cavity length; $a(t)$ is the law of laser cavity length modulation; φ is the initial phase.

The concentration C sought is determined as a function of amplitude of beatings on the dead (X_1) or the exit (Y_1) mirror:

$$C = \frac{1}{2\sigma L} \ln \frac{1}{X_1} A, \quad C = \frac{1}{2\sigma L} \ln \frac{1}{Y_1} B. \quad (2)$$

The coefficients A and B depend both on the lidar parameters and on the unperturbed quantities X_0 or Y_0 , which are determined on the corresponding mirrors; the expressions for A , B , X , and Y are given in Ref. 19.

The measured frequency, ν_b , of the intensity beatings at a saw-tooth modulation of the cavity length (ν_b^{\max} for a harmonic modulation) allows us to calculate the distance L to the target:

$$L = l \frac{\pi \nu_b^{\max}}{4\Omega} \frac{\lambda}{a_0} \quad \text{and} \quad L = \frac{l \nu_b \lambda}{2 \Omega a_0}, \quad (3)$$

where a_0 and Ω are the amplitude and frequency of the mirror vibrations.

Equation (2) enables us to estimate the expected frequency of beatings. Assume, for instance, that a CO₂-laser-based lidar with a 60-cm long cavity tracks a target at a distance of 10 km, and the mirror vibrates at 1 kHz frequency with the amplitude of 1 μm . Then, the frequency of beatings should be expected to be about 12.6 MHz. Note that in each particular case the modulation parameters must be chosen so that the frequency of beatings does not exceed the width of the passband cavity (this is especially important in long distance sensing).

Actually, Eqs. (1) to (3) are solutions of the inverse problem of remote sensing. Comparing two modulation schemes, one must conclude that the harmonic modulation has two obvious drawbacks. The first one is that in this case we have to deal with short time intervals near the time the mirror passes the point of equilibrium, to filter out the maximum frequency of beatings, ν_b^{\max} , while at saw-tooth modulation, the beatings' frequency is stable and we avoid dealing with a broad signal spectrum. The second and probably a minor drawback consists in that the maximum beating frequency, ν_b^{\max} , at the harmonic modulation is higher than the stable frequency, ν_b , at the saw-tooth modulation (we assume a_0 and Ω identical in both cases).

This difference, however, may become important, when it is needed to measure long distances. Indeed, these frequencies are related as follows:

$$\nu_b^{\max} / \nu_b = \pi / 2. \quad (4)$$

For example, if the distance L is about 300 km, $a_0 = 0.2 \mu\text{m}$, and the mirror vibration frequency is 0.25 kHz, then $\nu_b^{\max} \approx 30$, and $\nu_b \approx 19$ MHz.

It is worthy to note that at the point, where the mirror changes direction of its motion, at a saw-tooth modulation, there occurs a break of the phase of the laser intensity oscillations (Figs. 2a and b), which can complicate signal averaging.

An example of a numerical solution for a signal of an autodyne lidar at the harmonic modulation is shown in Fig. 2c. This solution well agrees with the experimentally measured signals^{14,22} and allows us to optimize the laser radar operation.

We must take into account that actually, in vertical sensing the concentration of the analyzed gas can vary along the sounding path. According to the barometric equation, air density decreases exponentially, so it is reasonable to apply the same function to the gases well mixed in the atmosphere, such as methane. For heavier gases the exponential dependence can also be used, but with a different value of the spatial scale β . To take into account the new regularity of signal attenuation in a gas, we must use the following formula instead of Eq. (1):

$$R'_0 = R_0 + \exp\left\{-\frac{2\sigma C_0}{\beta}(e^{-\beta a} - e^{-\beta L})\right\} \times \\ \times (1 - R_0)^2 R_2 \cos\left[\frac{\omega\tau}{l}a(t) + \varphi\right]. \quad (5)$$

Note that the coefficient $\exp(-\beta a)$ equals unity with a good accuracy, because the amplitude of mirror vibrations is about 1 μm , which, at the scale $1/\beta$ from several meters to several kilometers, gives $\beta a \sim 10^{-9} - 10^{-6}$. Hence, the expression for R'_0 is simplified:

$$R'_0 = R_0 + \exp\left\{-\frac{2\sigma C_0}{\beta}(1 - e^{-\beta L})\right\} \times \\ \times (1 - R_0)^2 R_2 \cos\left[\frac{\omega\tau}{l}a(t) + \varphi\right]. \quad (6)$$

Comparing it with Eq. (1), we see that the account of gas content fall off with height has yielded the coefficient $\exp\{-2\sigma C_0(1 - e^{-\beta L})/\beta\}$ in Eq. (6) instead of $\exp(-2\sigma CL)$ in Eq. (1). Since on a homogeneous path, CL is equal to the number N_{hom} of absorbing molecules per unit cross section of the beam, and on an inhomogeneous path the same number N_{inhom} equals $C_0(1 - e^{-\beta L})/\beta$, then it follows from comparison of Eqs. (1) and (6) that amplitudes of beatings depend, as should be expected, on the number of absorbing molecules only, and are not affected by their distribution along the sounding path.

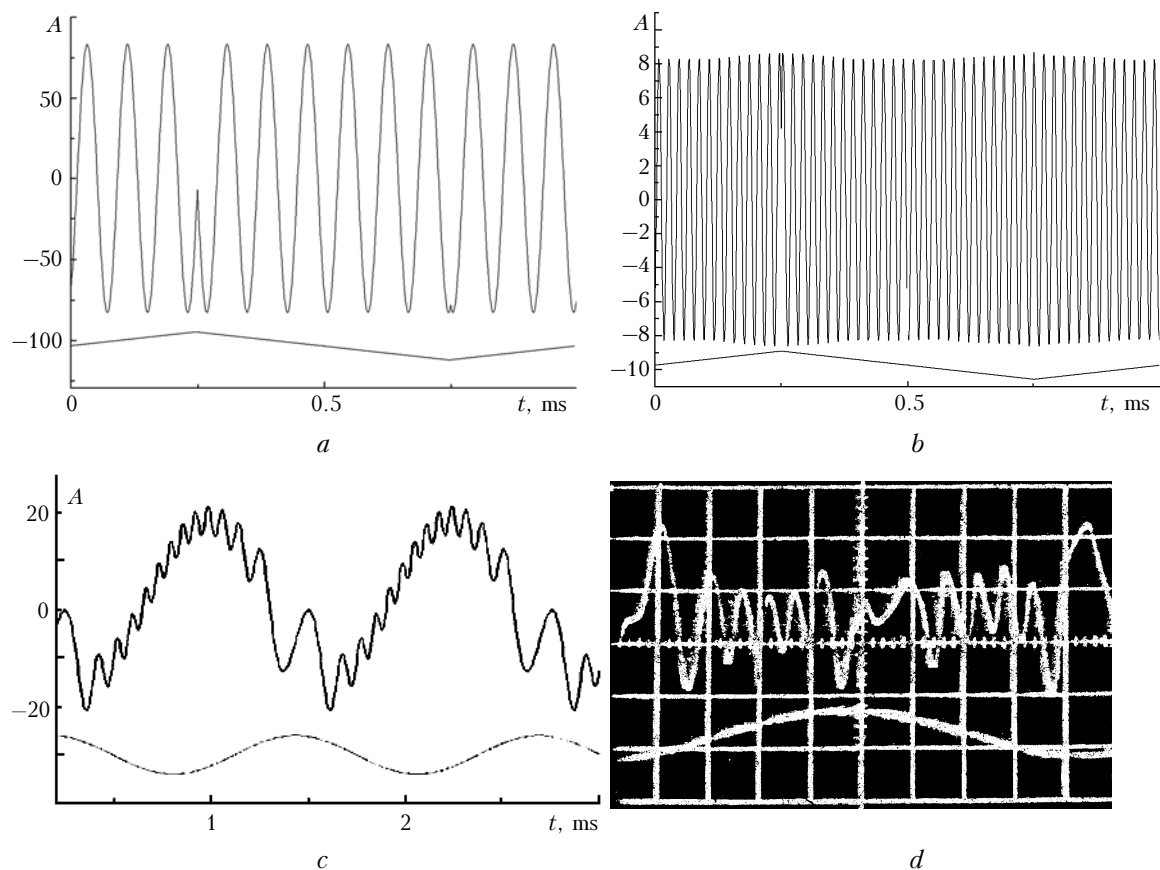


Fig. 2. Examples of numerical computations (*a–c*) and experimental records of the signal beatings (*d*). The lower curve depicts the position of the cavity mirror, the upper curve is the lidar signal in arbitrary units; the modulation frequency is 1 kHz (*a, b*) and 250 Hz (*c, d*); the sounding path is 10 (*a*) and 40-m long (*b, d*).

Depending on the vertical distribution of the absorbing molecules (the parameter β) and the height L the laser radar is at (this can be the cruising altitude of an aircraft carrier), the following variants are possible:

1. A uniformly mixed gas. In this case, β is known and gas concentration C_0 near the surface can easily be found.

2. A considered gas is a pollutant and is located in a thin layer of unknown thickness. In this case, lidar measurements can only give the total number of absorbing molecules along the sounding path.

3. A gas is sensed from a satellite. In this case, $\beta L \gg 1$, and it is possible to find the total number of absorbing molecules irrespective of the cruising altitude. The latter will only change the threshold sensitivity of measurements.¹⁷

Estimates of measurement sensitivity to concentrations of contaminating gases

A CO₂-laser-based autodyne lidar is a good means for remote measurements of concentrations of gaseous atmospheric pollutants by the differential

absorption method, because most of these gases absorb around 9–11 μm .

The least detectable gas concentration can be calculated by the equation derived in Ref. 14:

$$C_{\min} = \frac{\kappa}{2\Delta\sigma L_g(1-R_0)} \sqrt{\frac{h\nu\Delta f R_0}{P_0 r_{\text{eff}}}} \xi, \quad r_{\text{eff}} \approx T_{\text{tr}}^2 \frac{A S_t}{\pi L^2}, \quad (7)$$

where κ is the laser pump parameter; $\Delta\sigma$ is the difference between the absorption coefficients at the frequencies of sounding radiation $\text{cm}^{-1} \cdot \text{atm}^{-1}$; h is the Planck's constant; ν is the laser radiation frequency; Δf is the bandwidth of the electronic channel; P_0 is the intracavity generation power; ξ is the signal-to-noise ratio; r_{eff} is the effective reflectivity of the surface under study; T_{tr} is the transmittance of the optical path between the transmitter and receiver; A is the albedo of the reflector (a topographic object or the underlying surface); S_t is the area of the receiving telescope. Tables 1 and 2 give the values of C_{\min} (ppb in Table 1, ppm in Table 2) for some gases; for these estimates it is assumed that $\kappa = 0.36$, $R_0 = 0.85$, $P_0 = 10$ W, $S_t = 80$ cm², $\xi = 10$, $T_{\text{tr}} = 0.1$, $A = 0.04$; 0.5, $L_g = 20$ m.

Table 1. Horizontal path ($L = L_g, \Delta f = 1$ Hz)

Gas	Laser radiation parameter			$\Delta\sigma$	C_{\min}	
	Band	Transition	Frequency, cm^{-1}		$A = 0.04$	$A = 0.5$
CFCl_3	$00^0_1-02^0_0$	$R(22)$	1079.85	29.2	0.176	0.050
CF_2Cl_2	$00^0_1-10^0_0$	$P(32)$	932.96	35.7	0.133	0.038
C_2H_4	$00^0_1-10^0_0$	$P(14)$	949.48	31	0.155	0.044
C_2HCl_3	$00^0_1-10^0_0$	$P(20)$	944.19	12.6	0.380	0.108
$\text{C}_2\text{H}_3\text{Cl}$	$00^0_1-10^0_0$	$P(22)$	942.38	8.8	0.544	0.154
C_2Cl_4	$00^0_1-10^0_0$	$P(42)$	922.91	31	0.153	0.043
$\text{C}_2\text{Cl}_3\text{F}_3$	$00^0_1-02^0_0$	$P(26)$	104.28	21	0.240	0.068
$\text{C}_4\text{H}_5\text{Cl}$	$00^0_1-10^0_0$	$R(18)$	97.62	9.2	0.529	0.150
C_4H_8	$00^0_1-10^0_0$	$P(38)$	927.00	3.5	1.357	0.384
C_6H_6	$00^0_1-02^0_0$	$P(30)$	1037.43	2.5	2.010	0.568
NH_3	$00^0_1-02^0_0$	$R(30)$	1084.63	55.8	0.092	0.026
PH_3	$00^0_1-02^0_0$	$P(22)$	1045.02	1.7	2.966	0.839
O_3	$00^0_1-02^0_0$	$P(12)$	1053.92	12.2	0.415	0.117
N_2H_4	$00^0_1-10^0_0$	$P(22)$	942.38	2.7	1.773	0.502
$(\text{CH}_3)_2\text{N}_2\text{H}_4$	$00^0_1-10^0_0$	$P(30)$	934.89	2	2.385	0.674
$\text{CH}_3\text{N}_2\text{H}_4$	$00^0_1-10^0_0$	$R(30)$	982.10	1.38	3.542	1.002
HNO_3	$00^0_1-10^0_0$	$R(38)$	986.57	0.2	24.497	6.929
$^{13}\text{CO}_2$	$00^0_1-10^0_0$	$P(44)$	920.83	0.0015	3155.55	892.52
				S/N	$1.01 \cdot 10^5$	$3.58 \cdot 10^5$

Table 2. Vertical path ($L_g = 20$ m, $\Delta\theta = 10^{-3}$, $s = H$, $v = 150$ m/s for $H = 1.5$ km and $v = 8$ km/s for $H = 300$ km)

Gas	$H = 1$ km				$H = 5$ km				$H = 300$ km			
	Without scanning		With scanning		Without scanning		With scanning		Without scanning		With scanning	
	$A = 0.04$	$A = 0.5$	$A = 0.04$	$A = 0.5$	$A = 0.04$	$A = 0.5$	$A = 0.04$	$A = 0.5$	$A = 0.04$	$A = 0.5$	$A = 0.04$	$A = 0.5$
CFCl_3	0.107	0.030	3.399	0.961	0.240	0.068	7.601	2.150	0.430	0.122	30.404	8.600
CF_2Cl_2	0.082	0.023	2.584	0.731	0.183	0.052	5.779	1.635	0.327	0.092	23.115	6.538
C_2H_4	0.095	0.027	3.002	0.849	0.212	0.060	6.714	1.899	0.380	0.107	26.855	7.596
C_2HCl_3	0.233	0.066	7.366	2.084	0.521	0.147	16.472	4.659	0.932	0.264	65.887	18.636
$\text{C}_2\text{H}_3\text{Cl}$	0.333	0.094	10.537	2.980	0.745	0.211	23.562	6.664	1.333	0.377	94.247	26.657
C_2Cl_4	0.094	0.026	2.960	0.837	0.209	0.059	6.619	1.872	0.374	0.106	26.476	7.489
$\text{C}_2\text{Cl}_3\text{F}_3$	0.147	0.042	4.641	1.313	0.328	0.093	10.379	2.936	0.587	0.166	41.515	11.742
$\text{C}_4\text{H}_5\text{Cl}$	0.324	0.092	10.250	2.899	0.725	0.205	22.920	6.483	1.297	0.367	91.679	25.931
C_4H_8	0.831	0.235	26.276	7.432	1.858	0.526	58.756	16.619	3.324	0.940	235.023	66.474
C_6H_6	1.231	0.348	38.916	11.007	2.752	0.778	87.020	24.613	4.923	1.392	348.078	98.451
NH_3	0.056	0.016	1.783	0.504	0.126	0.036	3.986	1.128	0.226	0.064	15.946	4.510
PH_3	1.816	0.514	57.439	16.246	4.062	1.149	128.43	36.328	7.266	2.055	513.749	145.31
O_3	0.254	0.072	8.038	2.273	0.568	0.161	17.973	5.084	1.017	0.288	71.892	20.334
N_2H_4	1.086	0.307	34.343	9.714	2.428	0.687	76.794	21.721	4.344	1.229	307.176	86.882
$(\text{CH}_3)_2\text{N}_2\text{H}_4$	1.460	0.413	46.179	13.061	3.265	0.924	103.25	29.206	5.841	1.652	413.036	116.82
$\text{CH}_3\text{N}_2\text{H}_4$	2.169	0.614	68.595	19.402	4.850	1.372	153.38	43.383	8.677	2.454	613.531	173.53
HNO_3	15.001	4.243	474.38	134.17	33.544	9.488	1060.7	300.02	60.005	16.972	4242.98	1200.1
S/N	828	2930	26.2	92.5	370	1310	11.7	41.4	207	732	2.93	10.3

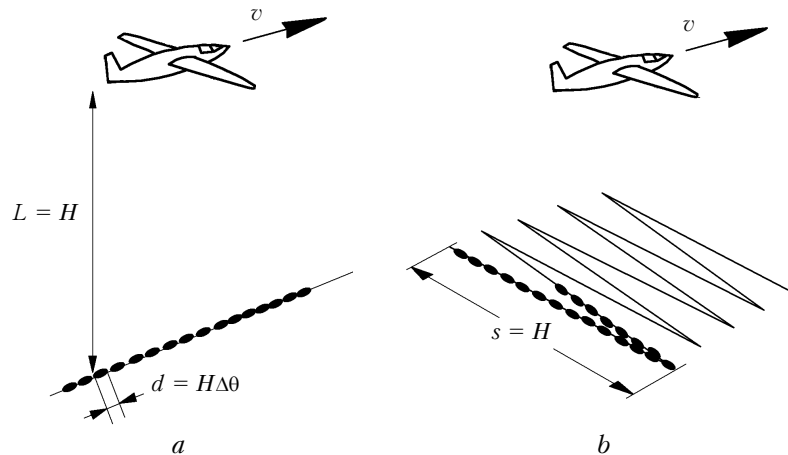


Fig. 3. The scheme of vertical sensing: without transverse scanning (a); with transverse scanning (b).

For the vertical path in Fig. 3, $\Delta f = v/(H\Delta\theta)$ without and $\Delta f = vs/(H\Delta\theta)^2$ with a transverse scanning (v is the speed of the carrier; H is its cruising height; $\Delta\theta$ is the beam divergence; s is the width of the scanning band).

Conclusion

Based on theoretical description of autodyne laser radar we have found the possibilities of calculating the concentrations of some pollutants and greenhouse gases by the differential absorption method. The following cases are considered: horizontal sensing, sensing of the near-surface layers from an aircraft carrier from altitudes of 1 and 5 km both with and without transverse scanning, and sensing from a satellite. The results obtained for the lidar with the telescope having a receiving optics area of 80 cm² prove that on the horizontal path the threshold detecting sensitivity for all the considered gases (except for ¹³CO₂) is less than 10–100 ppb, i.e., below their maximum permissible concentration. On the vertical path without scanning, the lowest detectable concentrations are 0.1–3 ppm. With scanning, the sensitivity for (CH₃)₂N₂H₄, CH₃N₂H₄, and HNO₃ worsens to 100–1000 ppm and for other substances to 3–50 ppm.

All this opens up the possibility of creating new generation of airborne and (in future) satellite-based gas-analyzing lidars capable of routinely monitoring large number of gases (including especially hazardous ones) over vast territories for the purposes of environmental management, mineral and other resource exploration, monitoring of production (and transportation) of hazardous substances, etc.

The main barrier that actually does not allow extension of the detection limits of autodyne laser radars is related to the transverse scanning. The most realistic way to increase lidar sensitivity is to increase the receiving telescope diameter and the output laser power.

Acknowledgments

This work was supported by INTAS-ESA (No. INTAS-99-822).

References

1. P.G.R. King and G.J. Steward, *New Science* **17**, No. 2, 180–185 (1963).
2. M. Harris, R. Loudon, G.L. Mander, and J.M. Vaughan, *Phys. Rev. Lett.* **67**, 1743 (1991).
3. A.P. Godlevskii, E.P. Gordov, A.Z. Fazliev, Ya.Ya. Ponurovskii, and P.P. Sharin, *Appl. Opt.* **26**, No. 8, 1607–1611 (1987).
4. E.P. Gordov, *Atmos. Oceanic Opt.* **8**, Nos. 1–2, 137–144 (1995).
5. S.F. Lukyanenko, M.M. Makogon, and L.N. Sinita, *Intracavity Laser Spectroscopy. Basics and Applications* (Nauka, Novosibirsk, 1985), 121 pp.
6. E.P. Gordov and G.S. Khmel'nitskii, *Atmos. Oceanic Opt.* **7**, No. 1, 63–64 (1994).
7. E.P. Gordov, G.S. Khmel'nitskii, and A.Z. Fazliev, *Proc. SPIE* **2773**, 160–163 (1996).
8. J. Churnside, E.P. Gordov, and A.V. Khachaturyan, *Technical Digest on Coherent Laser Radar: Technol. and Appl.* OSA **12**, 198 (1991).
9. E.P. Gordov, V.M. Orlovskii, A.G. Poteryaev, A.V. Khachaturyan, and J. Churnside, *Atmos. Oceanic Opt.* **6**, No. 4, 267–269 (1993).
10. E.P. Gordov and A.Z. Fazliev, *Atmos. Oceanic Opt.* **6**, No. 4, 283–284 (1993).
11. E.P. Gordov, *Proc. ESA Doppler Wind Lidar Workshop*, WPP-095, pp. 261–265.
12. E.P. Gordov, M.M. Makogon, A.Z. Fazliev, and V.M. Orlovskii, in: *Proc. of the 9th Conference on Coherent Laser Radar* (Linköping, Sweden, 1997), pp. 277–279.
13. M.M. Makogon, A.Z. Fazliev, and V.M. Orlovskii, *Proc. SPIE* **3485**, 583–591 (1998).
14. P.P. Sharin, "Studying possibilities of sounding atmospheric parameters based on intracavity effects in CO₂ laser," *Cand. Phys.-Math. Sci. Dissert.*, Tomsk (1992).
15. A.P. Godlevskii, E.P. Gordov, A.I. Zhiliba, and P.P. Sharin, *Atmos. Oceanic Opt.* **3**, No. 1, 20–24 (1990).
16. E.P. Gordov, G. Kaganov, and M.M. Makogon, in: *Proc. of Conf. on Measurement, Modeling, and Information Systems as Environmental Rehabilitation Tools* (Tomsk, 2000), pp. 21–23.
17. E.P. Gordov, M.M. Makogon, G. Kaganov, A.Z. Fazliev, and G.G. Matvienko, in: *11th Coherent Laser Radar Conference* (Malvern, Worcestershire, UK, 2001), pp. 60–63.
18. V.V. Zuev, M.Yu. Kataev, M.M. Makogon, and A.A. Mitsel, *Atmos. Oceanic Opt.* **8**, No. 8, 590–608 (1995).
19. G.A. Koganov, R. Shuker, and E.P. Gordov, *Appl. Opt.* **41**, No. 33, 7087–7091 (2002).
20. G.A. Koganov, R. Shuker, E.P. Gordov, and M.M. Makogon, *Invited Paper in Proc. of Intern. Conf. on Environm. Observat. Modeling and Information Systems as Tools for Urban/Regional Pollution Mitigation: ENVIROMIS-2002* (Tomsk, Russia, 2002), Vol. 1, pp. 24–27.
21. A.M. Khazanov, G.A. Koganov, and E.P. Gordov, *Atm. Opt.* **2**, No. 8, 717–722 (1989).
22. J.H. Churnside, *Appl. Opt.* **23**, No. 1, 61–66 (1984).
23. V.G. Goldort, E.P. Gordov, V.N. Ishchenko, A.A. Kovalev, and M.M. Makogon, *Atmos. Oceanic Opt.* **19**, Nos. 2–3, 187–188 (2006).